IOP Publishing J. Neural Eng. 18 (2021) 046089 https://doi.org/10.1088/1741-2552/ac0864

Journal of Neural Engineering

PAPER

Semantic verbal fluency brain network: delineating a physiological basis for the functional hubs using dual-echo ASL and graph theory approach

André Monteiro Paschoal[1,2,*], Pedro Henrique Rodrigues da Silva[2], Carlo Rondinoni[2], Isabella Velloso Arrigo[2], Fernando Fernandes Paiva[3] and Renata Ferranti Leoni[2]

[1] LIM44, Instituto e Departamento de Radiologia, Faculdade de Medicina, Universidade de Sao Paulo, Sao Paulo, Brazil
[2] Inbrain Lab, Department of Physics, FFCLRP, University of Sao Paulo, Ribeirao Preto, Brazil
[3] Institute of Physics of Sao Carlos, University of Sao Paulo, Sao Carlos, Brazil
[*] Author to whom any correspondence should be addressed.

E-mail: andre.paschoal@usp.br

RECEIVED
26 November 2019

REVISED
28 May 2021

ACCEPTED FOR PUBLICATION
4 June 2021

PUBLISHED
22 June 2021

Keywords: brain connectivity, cerebral blood flow, dual-echo readout, functional ASL, language network

Supplementary material for this article is available online

Abstract

Objective. Semantic verbal fluency (SFV) is a cognitive process that engages and modulates specific brain areas related to language comprehension and production, decision making, response inhibition, and memory retrieval. The impairment of the brain network responsible for these functions is related to various neurological conditions, and different strategies have been proposed to assess SVF-related deficits in such diseases. In the present study, the concomitant changes of brain perfusion and functional connectivity were investigated during the resting state and SVF task performance. *Approach*. Arterial spin labeling (ASL), a perfusion-based magnetic resonance imaging (MRI) method, was used with a pseudocontinuous labeling approach and dual-echo readout in 28 healthy right-handed Brazilian Portuguese speakers. The acquisition was performed in a resting state condition and during the performance of a SVF task. *Main results*. During task performance, a significant increase in cerebral blood flow (CBF) was observed in language-related regions of the frontal lobe, including Brodmann's areas 6, 9, 45, and 47, associated with semantic processing, word retrieval, and speech motor programming. Such regions, along with the posterior cingulate, showed a crucial role in the SVF functional network, assessed by seed-to-voxel and graph analysis. Our approach successfully overcame the generalization problem regarding functional MRI (fMRI) graph analysis with cognitive, task-based paradigms. Moreover, the CBF maps enabled the functional assessment of orbital frontal and temporal regions commonly affected by magnetic susceptibility artifacts in conventional T2*-weighted fMRI approaches. *Significance*. Our results demonstrated the capability of ASL to evaluate perfusion alterations and functional patterns simultaneously regarding the SVF network providing a quantitative physiological basis to functional hubs in this network, which may support future clinical studies.

1. Introduction

Verbal fluency (VF) is a cognitive function that allows retrieving specific semantic or phonemic information within restricted searching parameters [1, 2]. More specifically, semantic verbal fluency (SVF) typically involves generating words belonging to a given category. The cognitive processing associated with the SVF is supposed to engage and modulate specific brain areas related to language comprehension and production, decision making, response inhibition, and memory retrieval [3]. The impairment of the brain network responsible for these functions is related to several neurological conditions, such as Alzheimer's disease [4], Parkinson's disease [5], attention-deficit/hyperactivity disorder [6], epilepsy [7], and schizophrenia [8]. Therefore, different strategies have been employed to assess SVF-related

deficits related to them. They include the applications of neuropsychological tests [9] and neuroimaging techniques [3] in both clinical and investigational domains.

Functional neuroimaging studies have demonstrated the specialization of brain areas, mainly in frontal, parietal, and temporal lobes, for SVF processing [10, 11]. A recent meta-analysis reported left frontal areas along with left anterior cingulate (AC), thalamus, and precuneus as the central regions involved with word production, attentional demands, and working memory [3]. Other studies have also discussed the role of the temporal cortex, which is believed to mediate semantic-based word retrieval [11, 12]. A recent study confirmed its involvement with SFV in investigating the effects of cortical excitability modulation with transcranial direct current stimulation [13]. However, more than locating SFV-related regions, it is desirable to investigate how they are integrated. A dual-stream model consisted of ventral and dorsal pathways for language proposed that the dorsal route, which connects regions of the frontal lobe, is restricted to sensory-motor mapping of sound to articulation. In contrast, the ventral pathway, connecting the middle temporal lobe and the prefrontal cortex, subserves linguistic processing of sound to meaning [14]. The ventral regions are also highly connected during resting-state, representing a semantic network and facilitating neuronal activation during semantic-based tasks [15].

Moreover, recent studies have used graph theory analysis (GTA) to assess the topology of brain networks. They have reported that semantic, phonological, and orthographic networks have small-world characteristics defined by short average path lengths between nodes and high local clustering [16]. Regions of the anterior temporal lobe and inferior frontal cortex, including Broca's area, were reported as hubs in functional brain networks related to language processing [17, 18]. Also, graph analysis seems likely to become clinically relevant in neurology and psychiatry. It was useful to differentiate between mild cognitive impairment and Alzheimer's disease and assess atypical hemispheric dominance in brain tumors, evaluating functional connections in the language-related network [19, 20].

Many SVF studies have used functional magnetic resonance imaging (fMRI) based on the blood oxygen level-dependent (BOLD) contrast, given its fair compromise between spatial and temporal resolution and high sensitivity to neuronal-related hemodynamic changes [21]. However, BOLD contrast depends on a complex combination of blood oxygenation, cerebral blood volume, cerebral blood flow (CBF), and metabolic rate of oxygen, which may hinder the analysis of different diseases. On the other hand, assessing a single physiological parameter such as CBF, which is tightly coupled with glucose metabolism [22], is an appealing alternative for providing a novel perspective on the physiological basis underlying functional connectivity changes in the healthy and damaged brain.

Arterial spin labeling (ASL) has shown its advantages as a magnetic resonance (MR) perfusion-weighted technique. Besides being noninvasive, ASL shows tissue specificity [23] and, to some degree, is insensitive to susceptibility artifacts [24]. Perfusion-weighted images are achieved using the arterial blood as an endogenous tracer, magnetically labeled by the application of radiofrequency pulses. The pulses are applied in a strategic position (labeling plane), so the magnetization in the region of interest (ROI) is altered compared to a non-labeled condition [25, 26]. CBF is then estimated from the subtraction between unlabeled images (ASL control images) and labeled images. Due to the ASL intrinsic low signal-to-noise ratio, multiple unlabeled-label pairs are acquired and averaged to quantify CBF [27]. Moreover, the temporal series of ASL images allows the evaluation of CBF fluctuations over time, from which functional information can be estimated [21, 27, 28].

The investigation of the functional organization through ASL has two main advantages over BOLD-fMRI. First, ASL provides quantitative information about a single physiologic parameter (CBF) [29, 30]. Second, ASL has a better spatial specificity to neuronal activity because its signal originates in the capillary bed [31–35]. However, it is not as sensitive to hemodynamic alterations as BOLD-fMRI. Therefore, simultaneous BOLD and ASL sequences have been proposed [36–38]. In this context, ASL, combined with a dual-echo readout (DE-ASL), is an emerging approach to optimize the acquisition aiming at both CBF quantification and functional analysis [39]. Acquisition using short echo time (TE) provides perfusion-weighted images, while the use of longer TE increases the effect of transversal relaxation ($T2^*$), typical of the BOLD contrast [27, 40]. The BOLD signal measured from ASL images is called the concurrent BOLD (ccBOLD).

Therefore, a simultaneous BOLD-CBF analysis was performed to assess the brain functional connectivity of the SVF-related network in healthy participants. Both cognitive and resting-state runs were used to evaluate brain connectivity changes, as evidenced by CBF and ccBOLD signals. A single perfusion-based ASL acquisition with dual-echo readout was used to ensure the same state during task engagement for BOLD and CBF responses. No similar study was previously reported for a cognitive task. Therefore, our objectives were to demonstrate the feasibility and advantages of performing this method to investigate the physiological basis underlying the functional organization of the SVF network; and investigate the alterations in the SVF network from resting-state to task performance. We

Table 1. Data acquisition parameters.

	3D T1W	DE-pCASL	M0	3D TOF	3D FLAIR
FOV (mm^2)	240 × 240	240 × 240	240 × 240	200 × 180	240 × 240
Spatial resolution (mm^2)	1 × 1	3.75 × 3.75	3.75 × 3.75	0.45 × 0.63	1 × 1
Slice thickness (mm)	1	5	5	1.1	3
Number of slices	180	20	20	96	180
TR (ms)	7	4000	4000	20	5000
TE (ms)	3.2	(TE1/TE2) 9/28	14	3.45	324.21
FA (degrees)	8	90	90	20	90
Labeling duration (ms)	—	1550	—	—	—
Post-labeling delay (ms)	—	1600	—	—	—
Total scan time (min)	5.98	(RS/task) 4.4/6.8	1.5	3.58	3.45

hypothesize that CBF and frontal cortex (FC) changes will mainly involve the classical word production SVF-related regions, such as the left frontal and temporal regions.

2. Material and methods

2.1. Subjects

Twenty-eight healthy right-handed Brazilian Portuguese speakers were recruited. Exclusion criteria included: abuse of alcohol or illicit drugs, verified by the CAGE questionnaire (O'Brien 2008); previous experience with the cognitive test within less than 6 months; language other than Portuguese; psychiatric disorders; the presence of partial or total carotid artery stenosis, unilateral or bilateral; the presence of brain injury from stroke or tumor; the presence of pacemaker or prosthesis incompatible with the MR environment; claustrophobia; visual deficits; and pregnancy. Gender, age, and education years were obtained from a demographic questionnaire. Cognitive status was assessed by the Mini-Mental State Examination—Expanded Version (MMSE-2EV) [41]. Participants showed no cognitive impairment (MMSE-2EV: 60 ± 6). The Ethics Committee of the institution approved the study, and all participants gave their written informed consent before participating in the study.

2.2. Image acquisition and protocol

Images were acquired on a 3T MRI scanner (Philips Healthcare, Best, Netherlands) equipped with a 32-channel receive head coil. The complete protocol consisted of 3D T1-weighted TFE images, DE-ASL images under resting state and task performance. Proton-density-weighted images (M0) and 3D-TOF (time of flight), and axial FLAIR (fluid-attenuated inversion recovery), which were acquired with clinical protocols of the institution to confirm the absence of arterial occlusions and brain lesions, respectively. The acquisition parameters for all the sequences are reported in table 1.

The experimental protocol was divided into two runs: one consisting of a block-designed paradigm alternating a SVF task and a control condition, and another consisting of a 6 min run at resting-state. For the task-based experiment [42], one category (among animals, colors, sports, and foods) was presented for each task block, and the participants were asked to think about words related to that category. During the control condition, participants were asked to read the months of the year presented randomly on a screen. Each block lasted 32 s (eight image volumes), totaling four blocks of rest and four blocks of tasks. Commands were developed in PsychoPy software [43] and presented on a monitor positioned in front of the MR scanner. Participants viewed the monitor through a mirror system placed on the head coil. During the resting-state run, participants were asked to stay still with their eyes open in the absence of any specific thought or intention. Instead of including a rest condition between the task and control blocks, we chose to run a separate resting-state sequence to compare the task condition with the classical resting-state fMRI.

2.3. Image preprocessing

Imaging preprocessing was performed using customized scripts in MATLAB (MathWorks, Natick, MA), SPM12 (www.fil.ion.ucl.ac.uk/spm), and an open-source toolbox for ASL images (ASLtbx) [44]. Preprocessing steps were applied to each participant's data separately. First, raw ASL images were head-motion corrected, considering the middle image of the time series as reference. No image dataset was excluded because of the incorrigible motion artifact. Then, ASL images were coregistered to M0 and T1-weighted anatomical images, followed by a temporal filtering (high pass > 0.04 Hz) and spatial smoothing using an isotropic Gaussian kernel (FWHM = 4 mm for CBF quantification and FWHM = 6 mm for functional analysis). Furthermore, T1-weighted anatomical images were segmented into gray matter, white matter, and cerebrospinal fluid (CSF).

2.4. CBF quantification

Perfusion maps were generated by subtracting unlabeled and label images acquired with the short TE (= 9 ms). Quantification was performed using the sinc subtraction for regional CBF

mapping, while a running pairwise subtraction was performed for functional analysis to increase the number of perfusion-weighted images in the time series [45]. Quantification was based on the General Kinetic Model [29] using the following parameters: blood longitudinal relaxation time (T1b) = 1650 ms; labeling efficiency = 0.85; blood/-tissue water partition coefficient (gray matter/white matter) = 0.98/0.84 g ml^{-1}; tissue T1 (gray matter-/white matter) = 1020/770 ms [46]. Finally, CBF time series and mean CBF map were normalized to the MNI standard space (resolution = 2 × 2 × 2 mm^3; matrix size: 79 × 95 × 79).

2.5. Functional localization analysis

Functional analysis for resting-state and task conditions was performed using the time series of CBF and ccBOLD. The latter was obtained from the residual $T2^*$ weighting of the ASL images acquired with long TE (= 28 ms), regressing out the paradigm of the labeling and unlabeled [−1, 1, …, −1, 1] from the label/unlabeled image series [47]. CBF and ccBOLD time series were detrended and band-pass filtered (0.01–0.07 Hz for CBF; 0.0078–0.1 Hz for ccBOLD) [37]. A standard principal component analysis was used together with the CompCor algorithm [48] to remove the signal of white matter and CSF.

A general linear model analysis using the FSL (http://fsl.fmrib.ox.ac.uk/fsl/fslwiki) was performed on each participant's data to check the activation map obtained from CBF and ccBOLD (p-FDR < 0.05). The resulting maps were then compared with an anatomical template derived from the meta-analysis of different language tasks and fMRI [3]. After overlapping the activated regions of our GLM maps and the template from the meta-analysis, six anatomical brain regions in the left hemisphere were coincident: superior frontal gyrus (SFG)—Brodmann area (BA) 6 and BA8; medial frontal gyrus (MFG)—BA6; inferior frontal gyrus (IFG)—BA9, BA45 and BA47. They were selected for further analysis along with the posterior division of the left middle temporal gyrus (pMTG)—BA21 and the posterior division of the left superior temporal gyrus (pSTG)—BA22. These regions are called SVF-related in the remaining of the text. Additionally, four nodes of the default mode network (DMN) and the cingulate gyrus (anterior and posterior divisions) were assessed (supplementary material—table 1 (available online at stacks.iop.org/JNE/18/046089/mmedia)). The additional regions were included due to the recent literature on SVF tasks [49].

The mean CBF value of each region was obtained for three conditions: resting-state, control, and SVF. A two-way ANOVA with repeated measures was performed to assess the effects of region and condition on CBF, considering significance at $p < 0.05$. A Tukey posthoc analysis was performed to evaluate CBF changes among conditions for each ROI, considering multiple comparisons and significance at $p < 0.05$. This statistical analysis was performed in R software [50].

A seed-to-voxel analysis was performed using CONN Toolbox [51], considering the SVF-related regions (supplementary material—table 1, regions 1–8) as seeds for the task-based data. First, CBF and ccBOLD were considered separately, and then the main effects of each one were analyzed to obtain a single map from both imaging modalities. For the three cases, a bivariate Pearson's correlation on r-values transformed to z-scores was performed. Significant correlations after correction for multiple comparisons and a cluster size cut-off (two-sided p-FDR < 10^{-11}, $k \geqslant 10$ for CBF and ccBOLD separately; two-sided p-FDR < 10^{-13}, $k \geqslant 10$ for CBF and ccBOLD main effects) were shown in a spatial map. Surface maps were plotted using the standard template of CONN toolbox, the Freesurfer fsaverage surfaces.

The laterality index to verify the hemispheric dominance of SVF function and the degree of clustering to assess the spatial layout of the obtained maps were calculated since meaningful processes tend to exhibit a well-defined spatial structure [52]. The laterality index was defined as LI = (VLH − VRH)/(VLH + VRH), where VLH and VRH are the numbers of significant voxels in the left and right hemispheres of the obtained spatial maps, respectively. Left (LI > LITH) and right (LI < −LITH) dominances were assessed considering an LI threshold (LITH) of 0.2 [53]. The degree of clustering was defined as DCi = Nclu/Ntot for each obtained cluster i, where Nclu is the number of significant voxels of cluster i, and Ntot is the total number of significant voxels in the spatial map [54].

2.6. Functional integration analysis

First, an ROI-to-ROI analysis was performed considering the CBF and ccBOLD data separately for both SVF task and resting-state conditions. Then, for a combined analysis of CBF and ccBOLD, the ROI-to-ROI analysis was performed considering both data (p-FDR = 0.05, two-sided). For all cases, a bivariate Pearson's correlation on r-values transformed to z-scores was performed and checked the significance correcting for multiple comparisons.

2.7. Inter-subject variability

The inter-subject variability was assessed for each condition (i.e. CBF-rest, ccBOLD-rest, CBF-task, and ccBOLD-task) in all activated regions. To calculate the variability, a correlation was performed between the time-series of each eight SVF-related ROIs and the seven remaining ROIs, which resulted in a vector of correlations for every ROI. Next, for all the ROIs, another correlation was done among the 28 subjects for all the conditions [55]. A two-way

ANOVA with repeated measurements was employed to assess the difference between the inter-subject variability in the different conditions. The significance level was considered $p < 0.05$ corrected for multiple comparisons using Tuckey's method.

2.8. GTA

Graph analysis was performed using the Graph toolbox implemented in CONN [51]. The topological structure of the functional brain network organization during the performance of the SVF task was analyzed to verify whether a small-world topology was satisfied for CBF, ccBOLD, and combined CBF and ccBOLD data. The determination of the cut-off threshold was performed based on the approach of a previously reported study [56], as well as the analysis was run in two different templates separately.

Template 1: ROIs previously used for functional integration analysis (supplementary material—table 1).

Template 2: Functional templates of the resting-state networks available in CONN toolbox and composed by the DMN, sensory-motor network (SMN), visual network, salience network (SAN), dorsal attention network, frontal-parietal network, language network (LAN), cerebellar network, and their subdivisions, totalizing 32 nodes (supplementary material—table 2). This template comprised a whole-brain network and was used for exploratory analysis of the brain organization during the SVF task.

The next step was constructing a weighted adjacency matrix for each template and thresholding them over a range of r-values in steps of 0.01. Since there is no consensus on the most accurate approach for such thresholding [57], the following criteria to define the r-value range [56] were considered. First, the experimental network should be fully connected, i.e. every node should be integrated into the network by at least one edge [58]. Second, the experimental network should meet the criteria for a small-world network, as expected from a group of young participants [59]. Finally, the experimental network should be as cost-efficient as possible, i.e. it should have the lowest connection density while keeping the same efficiency. Therefore, its wiring cost should not exceed the value of 0.5 [60].

The small-world network considering two main criteria was also analyzed. First, the range in which the global efficiency of the experimental network approximates the global efficiency of an equivalent random network and, second, when its local efficiency surpasses that of an equivalent random network [61]. The analysis considering all criteria described above was used to find the range of r-values (Fisher transformed) for thresholding. The following parameters were calculated over the obtained range: clustering coefficient, local efficiency, characteristic path length, global efficiency, degree, and betweenness centrality (BC) [61–63]. Nodes with degree and BC values at least one standard deviation above the average values for the network were considered hubs.

All graph metrics were compared to assess the differences between the resting-state and SVF task. First, variable homoscedasticity was tested with the Shapiro–Wilk normality test (two-sided $p < 0.05$). For normal variables, a parametric t-test for two independent means was used. For non-normal variables, it was used non-parametric Mann–Whitney U-test (two-sided $p < 0.05$).

3. Results

3.1. CBF changes

Figure 1 shows the mean CBF values for all ROIs comparing resting-state, control condition, and SVF task performance. No region showed CBF differences when comparing the control condition with the other two conditions (SVF and resting-state). CBF differences were significant between SVF and resting-state conditions for the SFG (SFG—BA8, $p = 0.0134$; BA6, $p = 0.0067$), MFG (MFG—BA6; $p = 0.0214$), and IFG (IFG—BA45, $p = 0.0061$; BA9, $p = 0.0256$; BA47, $p = 0.0025$).

3.2. Seed-to-voxel analysis

Functional maps obtained from ccBOLD (figure 2(a)) and CBF (figure 2(b)) showed responses mostly in the left hemisphere during the SVF task, confirming the lateralization of this function. Responses were more lateralized for ccBOLD (LI = 0.65) compared to CBF (LI = 0.46), but no difference was observed regarding degree of clustering (CBF − DC = 0.017, ccBOLD − DC = 0.022; $p > 0.05$). Moreover, ccBOLD map showed a more extended response in the parietal lobule, while the CBF map showed a more extended response in the middle temporal gyrus, Heschl's gyrus, planum temporale, and insular cortex. When considering CBF and ccBOLD information simultaneously (figure 2(c)), it resulted in left lateralization (LI = 0.47) and degree of clustering similar to the other maps (DC = 0.018).

3.3. ROI-to-ROI analysis

Figure 3 shows the functional connectivity patterns for the SVF network compared to the resting-state (SVF task > resting-state). Results from ccBOLD (figure 3(a)) showed the IFG (BA9) connected to the Broca's area (IFG—BA47) and the posterior portion of the superior temporal gyrus. Moreover, connections among DMN regions were observed. Functional connectivity obtained from CBF (figure 3(b)) showed the AC connected to pMTG and PC. Finally, the SVF-related network, when considering the main effects of CBF and ccBOLD together (figure 4), showed the IFG-BA9 as an essential node, connecting

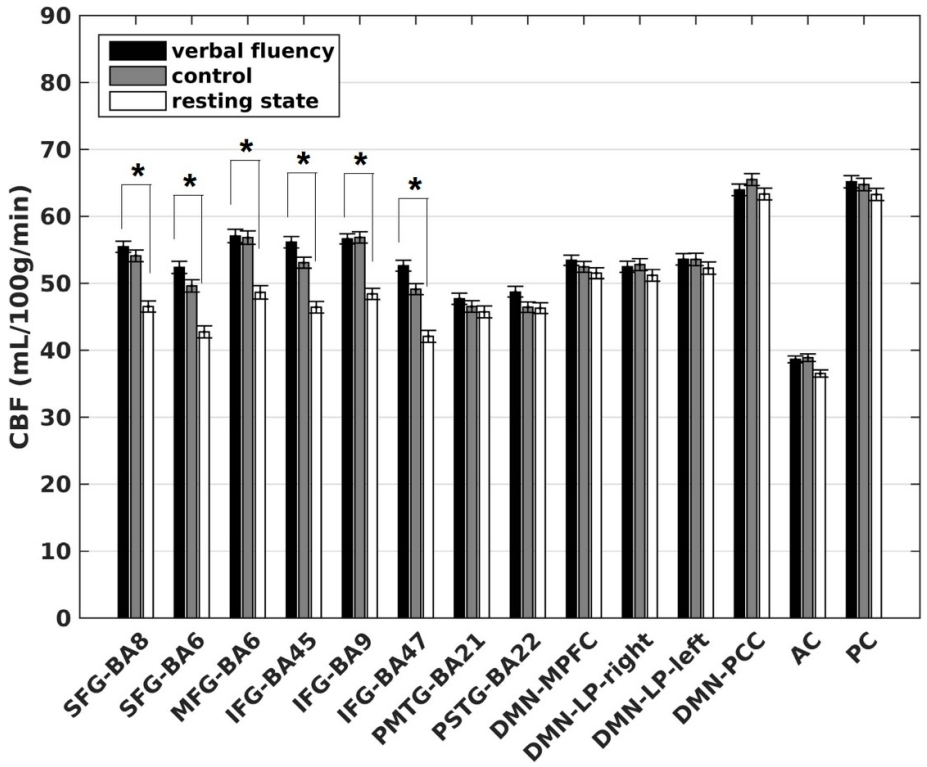

Figure 1. Regional CBF. Mean CBF values (ml/100 g min^{-1}) of each ROI for SVF (black), control (gray), and resting-state (white) conditions. A two-way ANOVA with repeated measures was performed to assess the effects of region and condition on CBF. A Tukey posthoc analysis was performed to assess CBF changes among conditions for each ROI. $^{*}p < 0.05$, corrected for multiple comparisons. SFG: superior frontal gyrus, MFG: medial frontal gyrus, IFG: inferior frontal gyrus, pMTG: middle temporal gyrus—posterior division, pSTG: superior temporal gyrus—posterior division, DMN: default mode network. MPFC: medial prefrontal cortex, LP: lateral parietal, PCC: posterior cingulate cortex, AC: anterior cingulate, PC: posterior cingulate.

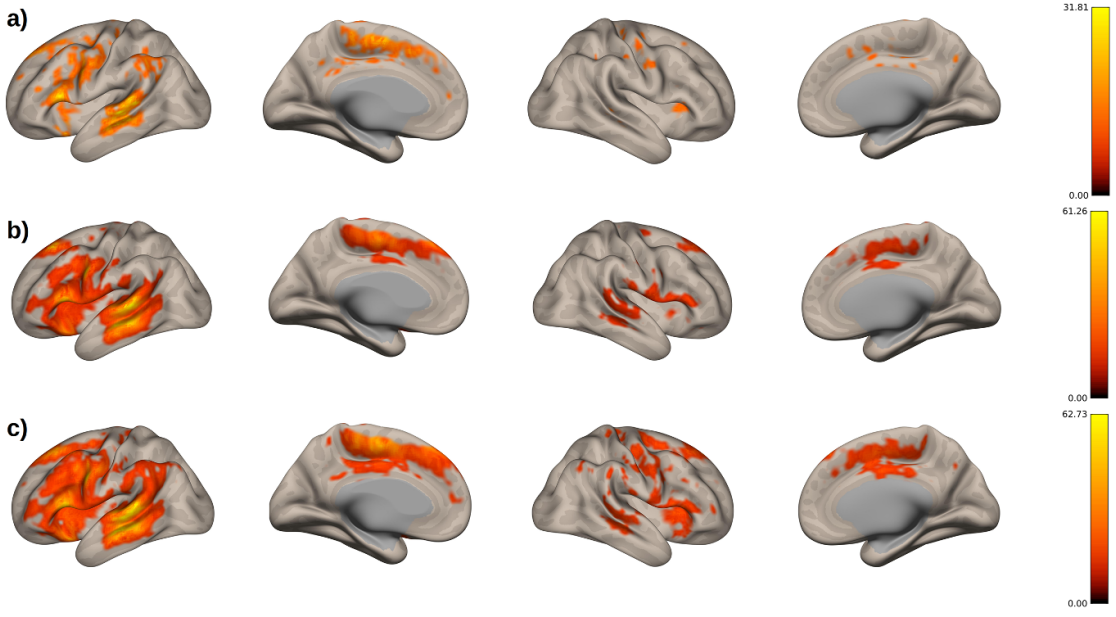

Figure 2. Functional localization. Functional maps of the SVF task for (a) ccBOLD (p-FDR $< 10^{-11}$, $k \geqslant 10$), (b) CBF (p-FDR $< 10^{-11}$, $k \geqslant 10$) and (c) combined CBF and ccBOLD time series (p-FDR $<10^{-13}$, $k \geqslant 10$). Color bars represent *F*-values.

inferior frontal and temporal regions and the connections among DMN regions. This conjunction analysis showed a more integrated network when compared to the findings depicted in figure 3.

3.4. Inter-subject variability

Figure 5 shows the mean inter-subject variability values for all SVF-related ROIs comparing the CBF and ccBOLD time-series for task and resting-state

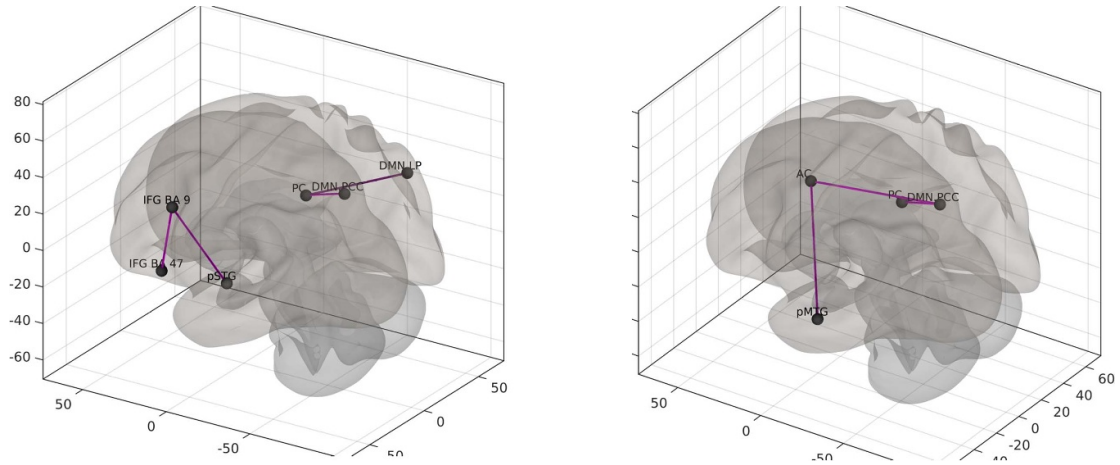

Figure 3. Functional connectivity. ROI-to-ROI functional connectivity patterns for (a) ccBOLD, and (b) CBF. Significance was set to $p < 0.05$, FDR-corrected (two-sided for ccBOLD and one sided for CBF).

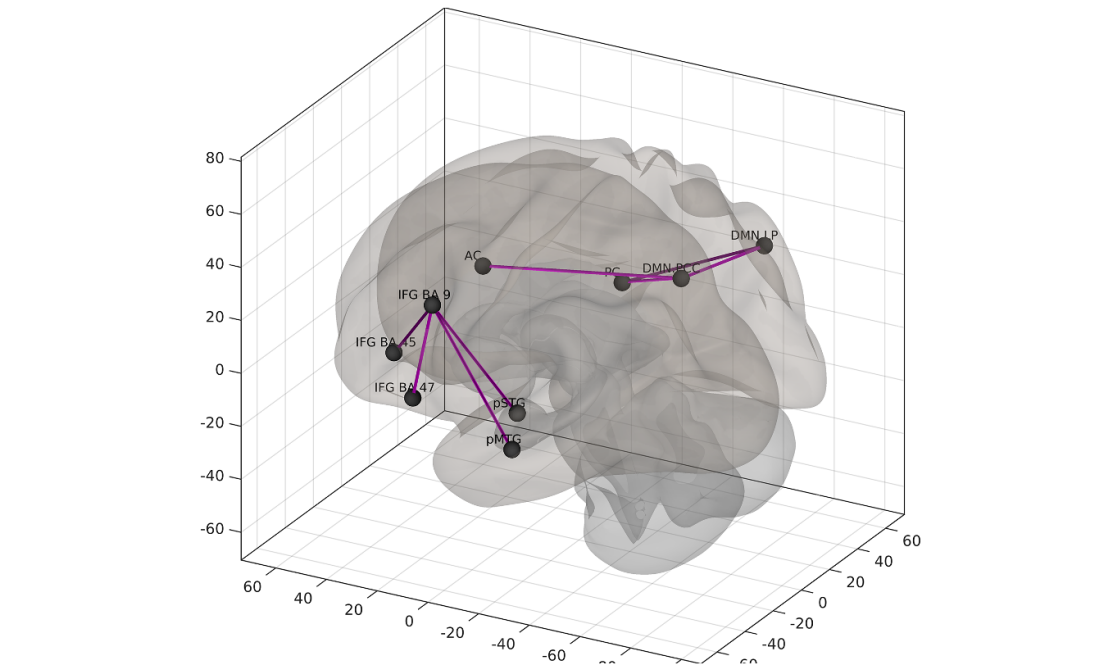

Figure 4. Functional integration. Functional connectivity pattern considering the main effects of CBF and cc-BOLD time series. All regions of template 1 were considered (supplementary material—table 1) (p-FDR < 0.05, two-sided).

conditions. Differences in the variability were significant between CBF-task and all other conditions for SFG—BA8; ccBOLD-task and all other conditions for MFG—BA6; between CBF-task and CBF-rest and ccBOLD-task for IFG—BA45; CBF-rest and CBF-task for IFG—BA47; and between ccBOLD-rest and CBF-rest and ccBOLD-task.

4. Graph analysis

4.1. Small-world networks

During resting-state and SVF tasks, our empirical data network met all criteria for small-worldness when considering CBF, ccBOLD, and CBF-ccBOLD time series for both templates. Table 2 presents the respective *r*-value ranges for such cases. For illustration, figure 6 shows the obtained graphs for combined CBF-ccBOLD data, indicating the intervals of costs where the networks present small-world characteristics when template 2 was used.

4.2. Graph metrics

Table 3 presents the graph metrics calculated from data obtained with CBF, ccBOLD, and the combination of CBF and ccBOLD information for both resting-state and task conditions, using templates 1 and 2, and the respective *r*-value ranges obtained for small-wordness criteria (table 2).

For template 1, local and global efficiency, degree and cost decreased significantly when considering

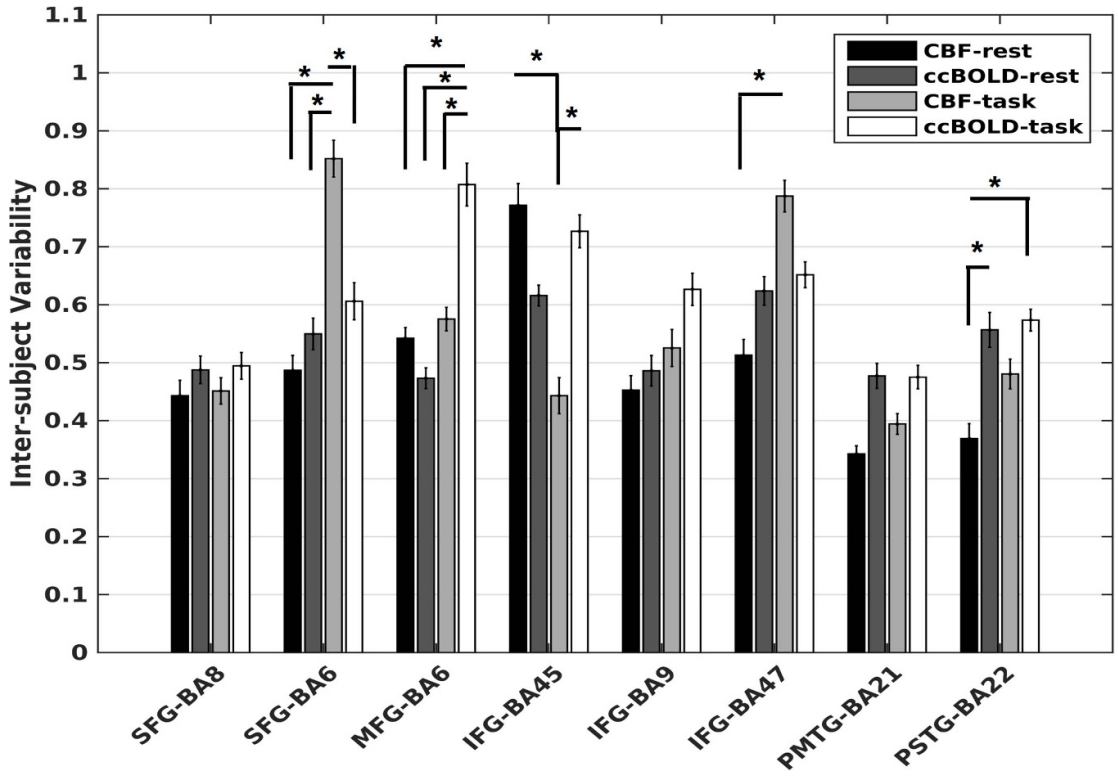

Figure 5. Inter-subject variability. Mean inter-subject variability of each ROI for CBF-rest (black), ccBOLD-rest (dark gray), CBF-task (light gray) and ccBOLD-task (white) conditions. A two-way ANOVA with repeated measures was performed to assess the effects of region and condition on inter-subject variability. A Tukey posthoc analysis was performed to assess CBF changes among conditions for each ROI. $^{*}p < 0.05$, corrected for multiple comparisons.

Table 2. *R*-value ranges, where the empirical data shows small-world characteristics.

	Resting-state condition				SVF task			
	Template 1		Template 2		Template 1		Template 2	
	*r*_min	*r*_max	*r*_min	*r*_max	*r*_min	*r*_max	*r*_min	*r*_max
ccBOLD	0.35	0.52	0.31	0.50	0.41	0.52	0.37	0.58
CBF	0.32	0.35	0.26	0.46	0.34	0.40	0.31	0.56
CBF-ccBOLD	0.32	0.39	0.29	0.46	0.38	0.46	0.35	0.56

*r*_min: minimum *r*-value; *r*_max: maximum *r*-value.

the CBF time-series, while all graph metrics showed statistically significant differences when considering CBF-ccBOLD time-series conjointly. For template 2, when combining both imaging categories, the global efficiency, BC, and cost decreased significantly, while the average path length and degree increased when comparing the resting-state condition and the SVF task performance.

Moreover, for template 2, regions that constitute the SMN, LAN established hubs during the resting-state condition, while regions of the DMN, SAN, LAN were hubs during task performance (table 4). The left IFG portion of LAN englobes part of the IFG-BA47 node, while both the superior node of SMN overlap with part of the SFG-BA6. In contrast, no functional hubs were found for template 1 when using the three time series (CBF, ccBOLD, and the combination of both) (figure 7).

5. Discussion

In the present study, the SVF network in healthy controls was evaluated using a dual-echo ASL acquisition, allowing the quantification of CBF and functional connectivity assessment concomitantly, which provided a physiological basis to our functional findings.

When comparing task performance with the resting-state condition, an increase in CBF was observed in language-associated regions in the frontal lobe, mainly in the inferior (BA 9, 45, and 47) and superior (BA 6 and 9) frontal gyri. These areas are associated with semantic [46, 47, 64] and phonological processing [51] and encoding [37, 48]. Broca's area (IFG—BA45) is involved in generating words and working memory during tasks similar to ours [27, 29, 30]. Moreover, a PET study reported that SFG

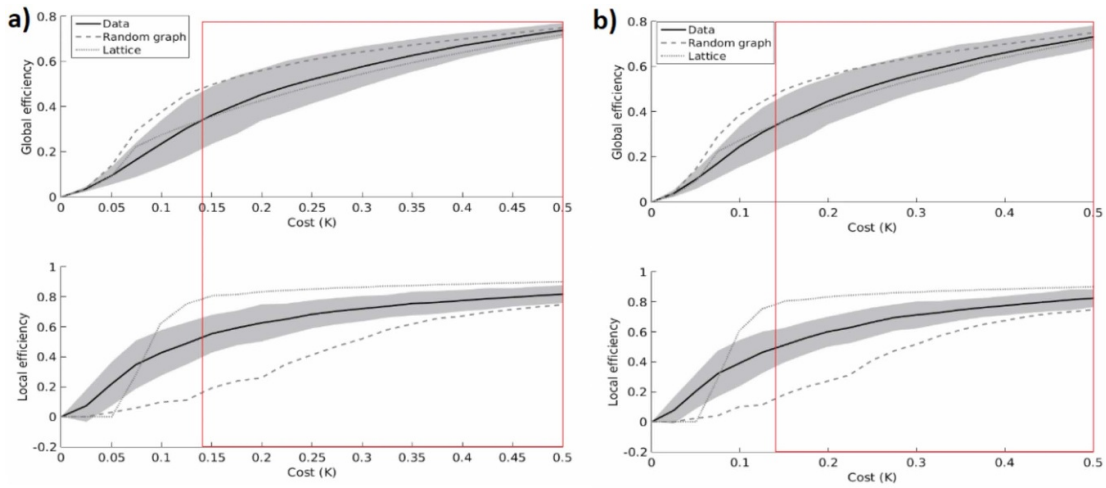

Figure 6. Small-world networks. Global efficiency and local efficiency versus the cost of the brain network organization (a) at resting-state and (b) task performance using template 2. Combined CBF-ccBOLD data was considered. Red rectangles indicate the regions where the networks present small-world characteristics.

is related to word retrieval [65], while a previous BOLD study reported its activation during an overt speech [66]. The significant CBF change in such a region during our covert word production task seems to be associated with word retrieval and speech motor programming. However, these areas did not show CBF increase when comparing the SVF task with the control condition, probably because these regions are also related to word reading, aloud or silently, as in our control task (reading the months of the year) [67, 68].

The functional connectivity maps obtained with the seed-to-voxel analysis showed similar spatial patterns when comparing CBF and ccBOLD data regarding left lateralization and response of the central SVF-related regions. However, the ccBOLD map showed response in a greater area of the superior frontal lobe and parietal lobule. These regions, associated with language processing and speech motor programming, were also found in CBF maps but in smaller clusters. On the other hand, the CBF map showed an extended response in the orbital part of the IFG and in the temporal gyrus, which encloses part of the LAN for comprehension and production, as identified in PET studies [58, 69]. Such areas are mostly affected by the signal loss at the interface of tissue and fluid/air due to local differences of magnetic susceptibility in conventional T2*-weighted fMRI approaches [17, 70]. The results obtained by DE-ASL overcame this issue, which suggests this method an appealing alternative to combine brain physiology and functionality in a non-invasive approach.

Additional connectivity findings include the anterior and posterior parts of the cingulate gyrus and parietal regions associated with transferring visual information to Wernicke's area and lexico-semantic processing of familiar words [71]. Moreover, the AC is activated during word generation and related to the task attentional demands. It was recently reported that this region is critical in reducing distraction from irrelevant stimuli and driving attention toward specific sites [72].

An ROI-to-ROI analysis evaluated the changes in brain temporal functional connectivity patterns between resting-state and SVF conditions. For ccBOLD, the IFG-BA9 appeared as a connecting region, as previously reported [9]. On the other hand, although CBF can represent a more spatial specific localization of activation sites [73, 74], there were fewer significant connections and nodes, which did not include the SFV-related regions in the inferior and superior frontal gyri. Such a feature reinforced the lower sensitivity of CBF for such measurements, presenting a limitation of using only CBF for ROI functional connectivity analysis during a cognitive task.

Moreover, the combined CBF-ccBOLD analysis presented two separate networks. One is composed of classical language-related regions, including Wernicke's area, where the information from the stimulus is comprehended, and phonological retrieval happens [74], then transferred to frontal areas words are generated [75]. The other network includes the posterior nodes of the DMN and the anterior and posterior portions of the cingulate cortex. Such a network may be related to aspects of memory retrieval [76] in mnemonical conditions. SVF functional organization presented small-world characteristics, i.e. high local and global efficiencies. It reflects highly clustered networks with a small average path length, allowing rapid communication between any two network regions [59]. As expected, the most probable functional hubs were found in regions of the language and sensorimotor networks when considering the whole brain (template 2).

Table 3. Graph metrics (mean ± SD) of the overall network for CBF, ccBOLD, and combined CBF-ccBOLD data.

Template 1									
	CBF			ccBOLD			CBF-ccBOLD		
	RS	Task	Statistics	RS	Task	Statistics	RS	Task	Statistics
Clustering coefficient	0.67 ± 0.19	0.63 ± 0.20	$U = 282, z = -1.79,$ $\dagger p = 0.07$	0.67 ± 0.15	0.69 ± 0.13	$t = 1.08, {}^{*}p = 0.28$	0.68 ± 0.18	0.62 ± 0.11	$U = 1059, z = -2.96,$ $\mathbf{\dagger p = 0.0031}$
Local efficiency	0.75 ± 0.21	0.70 ± 0.22	$U = 267, z = -2.04,$ $\mathbf{\dagger p = 0.041}$	0.75 ± 0.16	0.78 ± 0.13	$U = 351, z = 0.66,$ $\dagger p = 0.51$	0.76 ± 0.19	0.73 ± 0.11	$U = 1123, z = -2.59,$ $\mathbf{\dagger p = 0.0096}$
Global efficiency	0.645 ± 0.19	0.48 ± 0.24	$t = -2.85, \mathbf{{}^{*}p = 0.006}$	0.58 ± 0.21	0.61 ± 0.22	$t = 0.54, {}^{*}p = 0.59$	0.64 ± 0.21	0.51 ± 0.13	$U = 887, z = -3.96,$ $\mathbf{\dagger p = 0.00008}$
Average path length	1.79 ± 0.52	1.64 ± 0.26	$U = 357, z = -0.56,$ $\dagger p = 0.57$	1.73 ± 0.34	1.69 ± 0.36	$t = -0.45, {}^{*}p = 0.65$	1.67 ± 0.37	2.08 ± 0.32	$U = 647, z = 5.36,$ $\mathbf{\dagger p = 0.00001}$
BC	0.06 ± 0.04	0.04 ± 0.02	$U = 295, z = -1.58,$ $\dagger p = 0.11$	0.05 ± 0.02	0.05 ± 0.02	$t = -0.35, {}^{*}p = 0.73$	0.05 ± 0.02	0.03 ± 0.01	$t = -5.66,$ $\mathbf{{}^{*}p < 0.00001}$
Degree	5.89 ± 2.78	4.41 ± 2.83	$U = 268, z = -2.02,$ $\mathbf{\dagger p = 0.043}$	5.09 ± 2.57	5.55 ± 2.82	$t = 0.64, {}^{*}p = 0.52$	5.99 ± 2.84	8.86 ± 3.74	$t = 4.56,$ $\mathbf{{}^{*}p = 0.000013}$
Cost	0.45 ± 0.21	0.34 ± 0.22	$U = 268, z = -2.02,$ $\mathbf{\dagger p = 0.043}$	0.39 ± 0.20	0.43 ± 0.22	$t = 0.64, {}^{*}p = 0.52$	0.46 ± 0.22	0.29 ± 0.12	$t = -5.25,$ $\mathbf{{}^{*}p < 0.00001}$
Template 2									
	CBF			ccBOLD			CBF-ccBOLD		
	RS	Task	Statistics	RS	Task	Statistics	RS	Task	Statistics
Clustering coefficient	0.65 ± 0.10	0.63 ± 0.12	$t = -0.44, {}^{*}p = 0.66$	0.65 ± 0.10	0.66 ± 0.13	$t = 0.12, {}^{*}p = 0.91$	0.67 ± 0.20	0.64 ± 0.13	$U = 1316, z = -1.46,$ $\dagger p = 0.14$
Local efficiency	0.76 ± 0.09	0.74 ± 0.12	$U = 359, z = -0.53,$ $\dagger p = 0.59$	0.77 ± 0.09	0.77 ± 0.13	$U = 374, z = 0.29,$ $\dagger p = 0.77$	0.74 ± 0.22	0.75 ± 0.13	$U = 1412, z = -0.90,$ $\dagger p = 0.37$
Global efficiency	0.59 ± 0.11	0.54 ± 0.11	$t = -1.73, {}^{*}p = 0.089$	0.59 ± 0.12	0.56 ± 0.16	$t = -0.92, {}^{*}p = 0.36$	0.63 ± 0.22	0.55 ± 0.14	$U = 1113, z = -2.64,$ $\mathbf{\dagger p = 0.0083}$
Average path length	1.97 ± 0.35	2.01 ± 0.32	$t = 0.45, {}^{*}p = 0.65$	2.00 ± 0.45	1.91 ± 0.41	$U = 359, z = 1.51,$ $\dagger p = 0.13$	1.67 ± 0.39	1.97 ± 0.39	$U = 908, z = 3.84,$ $\mathbf{\dagger p = 0.00012}$

(Continued.)

Table 3. (Continued.)

	Template 2								
	CBF			ccBOLD			CBF-ccBOLD		
	RS	Task	Statistics	RS	Task	Statistics	RS	Task	Statistics
BC	0.03 ± 0.01	0.03 ± 0.01	$U = 377, z = -0.24,$ $\dagger p = 0.81$	0.03 ± 0.01	0.02 ± 0.01	$U = 299, z = -0.53,$ $\dagger p = 0.60$	0.05 ± 0.03	0.03 ± 0.01	$U = 907, z = -3.84,$ $\mathbf{\dagger p = 0.00012}$
Degree	10.6 ± 3.76	9.68 ± 3.91	$t = -0.95, {}^{*}p = 0.35$	10.78 ± 4.35	10.72 ± 5.40	$t = -0.05, {}^{*}p = 0.96$	5.92 ± 3.06	10.17 ± 4.92	$U = 757, z = 4.72,$ $\mathbf{\dagger p < 0.00001}$
Cost	0.34 ± 0.12	0.31 ± 0.13	$t = -0.95, {}^{*}p = 0.35$	0.35 ± 0.14	0.35 ± 0.17	$t = -0.05, {}^{*}p = 0.96$	0.46 ± 0.23	0.33 ± 0.16	$U = 1074, z = -2.87,$ $\mathbf{\dagger p = 00041}$

RS: resting-state; SD: standard deviation.

Compared to resting-state: $^{*}p$ calculated using the t-test for two independent means; $\dagger p$ calculated using Mann Whitney U-test. Significant differences in bold.

Table 4. Functional hubs obtained for template 2.

	Resting-state			Task		
	Region	BC	Degree	Region	BC	Degree
CBF	Left lateral (SMN)	0.050	16.30	Left Lateral (SMN)	0.043	14.63
	Right lateral (SMN)	0.047	16.00	Left SMG (SAN)	0.042	13.86
	Left pSTG (LAN)	0.053	16.35	Left pSTG (LAN)	0.051	15.17
ccBOLD + CBF	Left lateral (SMN)	0.048	13.50	Left pSTG (LAN)	0.049	15.13
	Right lateral (SMN)	0.046	13.19	—	—	—
	Left pSTG (LAN)	0.057	13.32	—	—	—

BC: betweenness centrality, SMN: sensory-motor network, LAN: language network, SAN: salience network. pSTG: posterior superior temporal gyrus, SMG: supramarginal gyrus.

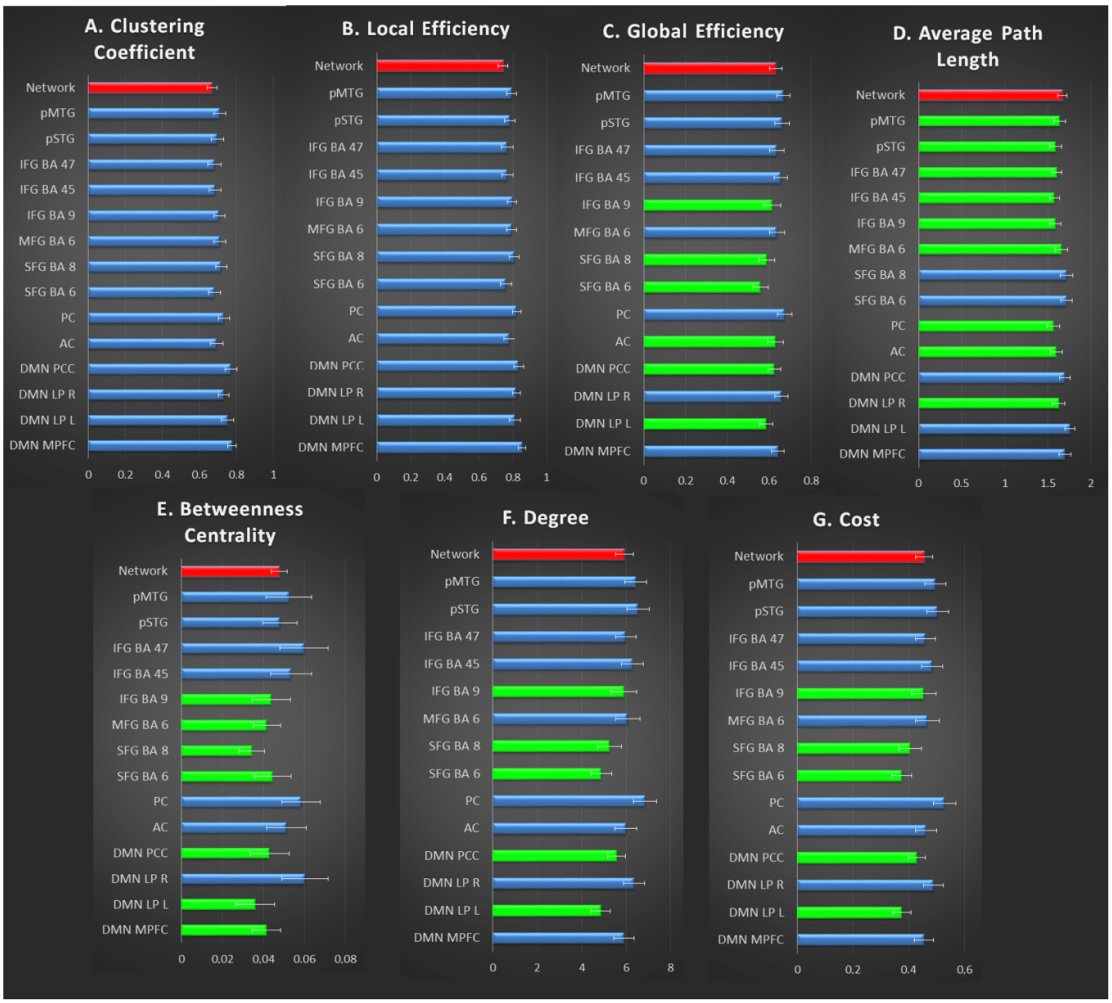

Figure 7. Graphs metrics. Panels (A)–(G) illustrate the averaged graph metrics of the SVF network considering the combined CBF-ccBOLD information (r-value range: 0.38–0.46) during task condition. Red: the network mean values; blue: regions with a mean value higher than the average value for the network; light green: regions with equal or smaller values than the average value for the network. Error bars represent the standard error. SFG: superior frontal gyrus, MFG: medial frontal gyrus, IFG: inferior frontal gyrus, pMTG: middle temporal gyrus—posterior division, pSTG: superior temporal gyrus—posterior division, DMN: default mode network. MPFC: medial prefrontal cortex, LP: lateral parietal, PCC: posterior cingulate cortex, AC: anterior cingulate, PC: posterior cingulate.

The analysis of inter-subject variability revealed noteworthy findings when comparing CBF and ccBOLD functional connectivity results. First, the classical language areas, namely Broca (BA45) and Wernicke (BA22), showed differences in variability between subjects across conditions, which probably points to the fact that under a language task, these key regions are engaged at most during processing. Furthermore, a lower inter-subject variability was found for CBF under task condition, pointing to a homogenous activity across the subjects. The variability can be justified considering that language can

be influenced by sex, education, cognitive strategy, or even physiological noise. Secondly, the regions whose CBF variation coincided with functional hubs (SFG-BA6 and IFG47), as observed in graph analysis results, also showed differences in variability across subjects. Beyond providing a physiological basis for SVF task-related functional hubs, the quantitative nature of the analysis and its lower inter-subject variability would make CBF fMRI a good technique for group comparisons.

Another approach used to verify the alterations in the whole-brain network from resting-state to task performance was the graph metrics. For this analysis, increases in the average path length and degree and decreases in the BC, global efficiency, and cost were observed when analyzing the combined CBF-ccBOLD. Previous resting-state fMRI studies pointed towards small-world topology [77], which is considered a characteristic of healthy subjects. However, graph analysis in task-based fMRI suffers from limited validity and generalization [41]. Therefore, we applied the criteria used in a previous GTA of language in the brain at rest [56] and found similar and consistent results.

In summary, the graph analysis using the CBF and BOLD information concomitantly and a whole-brain template for the nodes allowed us to assess the changes in the SVF functional network when comparing the resting-state condition with the task performance. Our results suggest that the used methodology may overcome the generalization problem regarding fMRI graph analysis with cognitive paradigms. Therefore, the graph theory approach can be used as a tool in future studies to assess functional markers between healthy and clinical groups in both rest and task-based fMRI if one carefully selects the regions of interest.

The joint CBF-ccBOLD analysis presented a more interconnected network with every node integrated with the network by at least one edge than ccBOLD and CBF individual findings. Interestingly, it meets the first criteria considered in this study to perform graph analysis [58]. It suggests that joint CBF-ccBOLD is useful to apply graph theory approaches. Additionally, it was possible to delineate a physiological basis for functional hubs in the SVF network once significant CBF changes in SFG-BA6 and IFG-47 nodes match areas of functional hubs of the SVF network namely the SMN and LAN networks. It suggests that dual-echo acquisition providing CBF and ccBOLD conjunction analysis helps determine functional hubs in task performance and its related physiological basis using a whole-brain parcellation template.

Limitations of our study include the relatively small number of participants, and the SVF task performed silently. Currently, VF fMRI studies have used loud articulation of words since silent articulation may produce non-linguistic activation, resulting from response inhibition within the motor speech system. However, we chose the silent performance of the SVF task to avoid motor and movement artifacts. Regarding the sample size, although small, it is similar to the number of participants of other task-based fMRI studies. Moreover, the results were consistent between subjects and were following what we expected based on the literature.

In conclusion, our study demonstrated the potential of the ASL technique to assess an important brain function by evidence of a quantitative physiological parameter. Through a single MRI acquisition, our results suggested the effectiveness of ASL to detect CBF changes under an SVF task and are comparable to other imaging techniques. Moreover, our CBF/ccBOLD results for network delineation, functional connectivity, and graph analysis provided a complete evaluation of the functional brain connectivity in agreement with classical literature results. The advantage of spatial specificity and quantitative physiological information makes ASL an appealing method to investigate neurological disorders that affect the cognitive processing of language-associated brain function.

Data availability statement

The data that support the findings of this study are available upon reasonable request from the authors.

Acknowledgments

This study was financed in part by the Coordenação de Aperfeiçoamento de Pessoal de Nível Superior—Brasil (CAPES)—Finance Code 001, and Conselho Nacional de Desenvolvimento Científico e Tecnológico—Process Number 140110/2016-0.

Author contributions

All authors designed the study, analyzed the results, and wrote the paper. A M P acquired all MRI data and performed the imaging pre- and post-processing and functional connectivity analysis. P H R S participated in the imaging post-processing and functional connectivity analysis and performed the graph analysis.

Conflict of interest

The authors declare no competing interests.

ORCID iDs

André Monteiro Paschoal https://orcid.org/0000-0001-8269-711X
Renata Ferranti Leoni https://orcid.org/0000-0002-4568-0746

References

[1] Lezak M D, Loring D W and Howieson D B 2004 *Neuropsychological Assessment* 5th (Oxford: Oxford University Press)1200

[2] Mascali D, DiNuzzo M, Serra L, Mangia S, Maraviglia B, Bozzali M and Giove F 2018 Disruption of semantic network in mild Alzheimer's disease revealed by resting-state fMRI *Neuroscience* **371** 38–48

[3] Wagner S, Sebastian A, Lieb K, Tuscher O and Tadic A 2014 A coordinate-based ALE functional MRI meta-analysis of brain activation during verbal fluency tasks in healthy control subjects *BMC Neurosci.* **15** 19

[4] Zhao Q, Guo Q and Hong Z 2013 Clustering and switching during a semantic verbal fluency test contribute to differential diagnosis of cognitive impairment *Neurosci. Bull.* **29** 75–82

[5] Pettit L, McCarthy M, Davenport R and Abrahams S 2013 Heterogeneity of letter fluency impairment and executive dysfunction in Parkinson's disease *J. Int. Neuropsychol. Soc.* **19** 986–94

[6] Andreou G and Trott K 2013 Verbal fluency in adults diagnosed with attention-deficit hyperactivity disorder (ADHD) in childhood *Atten. Defic. Hyperact. Disord.* **5** 343–51

[7] Metternich B, Buschmann F, Wagner K, Schulze-Bonhage A and Kriston L 2014 Verbal fluency in focal epilepsy: a systematic review and meta-analysis *Neuropsychol. Rev.* **24** 200–18

[8] Tyburski E, Sokolowski A, Chec M, Pelka-Wysiecka J and Samochowiec A 2015 Neuropsychological characteristics of verbal and non-verbal fluency in schizophrenia patients *Arch. Psychiatr. Nurs.* **29** 33–38

[9] Piskunowicz M, Bielinski M, Zglinski A and Borkowska A 2013 Verbal fluency tests—application in neuropsychological assessment *Psychiatr. Pol.* **47** 475–85

[10] Glikmann-Johnston Y, Oren N, Hendler T and Shapira-Lichter I 2015 Distinct functional connectivity of the hippocampus during semantic and phonemic fluency *Neuropsychologia* **69** 39–49

[11] Price C J 2010 The anatomy of language: a review of 100 fMRI studies published in 2009 *Ann. New York Acad. Sci.* **1191** 62–88

[12] Baldo J V, Schwartz S, Wilkins D and Dronkers N F 2006 Role of frontal versus temporal cortex in verbal fluency as revealed by voxel-based lesion symptom mapping *J. Int. Neuropsychol. Soc.* **12** 896–900

[13] Ghanavati E, Salehinejad M A, Nejati V and Nitsche M A 2019 Differential role of prefrontal, temporal and parietal cortices in verbal and figural fluency: implications for the supramodal contribution of executive functions *Sci. Rep.* **9** 3700

[14] Saur D *et al* 2008 Ventral and dorsal pathways for language *Proc. Natl Acad. Sci.* **105** 18035–40

[15] Wawrzyniak M, Hoffstaedter F, Klingbeil J, Stockert A, Wrede K, Hartwigsen G, Eickhoff S B, Classen J, Saur D and Stamatakis E A 2017 Fronto-temporal interactions are functionally relevant for semantic control in language processing *PLoS One* **12** e0177753

[16] Trautwein J and Schroeder S 2018 Orthographic networks in the developing mental lexicon. insights from graph theory and implications for the study of language processing *Front. Psychol.* **9** 2252

[17] Visser M, Jefferies E and Lambon Ralph M A 2010 Semantic processing in the anterior temporal lobes: a meta-analysis of the functional neuroimaging literature *J. Cogn. Neurosci.* **22** 1083–94

[18] Elmer S 2016 Broca pars triangularis constitutes a 'Hub' of the language-control network during simultaneous language translation *Front. Hum. Neurosci.* **10** 491

[19] Bertola L, Mota N B, Copelli M, Rivero T, Diniz B S, Romano-Silva M A, Ribeiro S and Malloy-Diniz L F 2014 Graph analysis of verbal fluency test discriminate between patients with Alzheimer's disease, mild cognitive impairment and normal elderly controls *Front. Aging Neurosci.* **6** 185

[20] Li Q, Dong J W, Del Ferraro G, Petrovich Brennan N, Peck K K, Tabar V, Makse H A and Holodny A I 2019 Functional translocation of Broca's area in a low-grade left frontal glioma: graph theory reveals the novel, adaptive network connectivity *Front. Neurol.* **10** 702

[21] Aguirre G K, Detre J A, Zarahn E and Alsop D C 2002 Experimental design and the relative sensitivity of BOLD and perfusion fMRI *Neuroimage* **15** 488–500

[22] Liang X, Zou Q, He Y and Yang Y 2013 Coupling of functional connectivity and regional cerebral blood flow reveals a physiological basis for network hubs of the human brain *Proc. Natl Acad. Sci.* **110** 1929–34

[23] Detre J A, Zhang W, Roberts D A, Silva A C, Williams D S, Grandis D J, Koretsky A P and Leigh J S 1994 Tissue specific perfusion imaging using arterial spin labeling *NMR Biomed.* **7** 75–82

[24] Petcharunpaisan S 2010 Arterial spin labeling in neuroimaging *World J. Radiol.* **2** 384–98

[25] Detre J A, Leigh J S, Williams D S and Koretsky A P 1992 Perfusion imaging *Magn. Reson. Med.* **23** 37–45

[26] Ferre J-C, Bannier E, Raoult H, Mineura G, Carsin-Nicol B and Gauvrit J-Y 2013 Perfusion par arterial spin labeling (ASL): technique et mise en œuvre clinique *J. Radiol. Diagn. Int.* **94** 1208–21

[27] Wong E C, Buxton R B and Frank L R 1997 Implementation of quantitative perfusion imaging techniques for functional brain mapping using pulsed arterial spin labeling *NMR Biomed.* **10** 237–49

[28] Talagala S L and Noll D C 1998 Functional MRI using steady-state arterial water labeling *Magn. Reson. Med.* **39** 179–83

[29] Buxton R B, Frank L R, Wong E C, Siewert B, Warach S and Edelman R R 1998 A general kinetic model for quantitative perfusion imaging with arterial spin labeling *Magn. Reson. Med.* **40** 383–96

[30] Buxton R B 2005 Quantifying CBF with arterial spin labeling *J. Magn. Reson. Imaging* **22** 723–6

[31] Detre J A and Wang J J 2002 Technical aspects and utility of fMRI using BOLD and ASL *Clin. Neurophysiol.* **113** 621–34

[32] Galazzo I B, Storti S F, Formaggio E, Pizzini F B, Fiaschi A, Beltramello A, Bertoldo A and Manganotti P 2014 Investigation of brain hemodynamic changes induced by active and passive movements: a combined arterial spin labeling-BOLD fMRI study *J. Magn. Reson. Imaging* **40** 937–48

[33] Galazzo I B, Storti S F, Del Felice A, Pizzini F B, Arcaro C, Formaggio E, Mai R, Chappell M, Beltramello A and Manganotti P 2015 Patient-specific detection of cerebral blood flow alterations as assessed by arterial spin labeling in drug-resistant epileptic patients *PLoS One* **10** 1–24

[34] Lu H Z, Donahue M J and van Zijl P C M 2006 Detrimental effects of BOLD signal in arterial spin labeling fMRI at high field strength *Magn. Reson. Med.* **56** 546–52

[35] Pimentel M A F, Vilela P, Sousa I and Figueiredo P 2013 Localization of the hand motor area by arterial spin labeling and blood oxygen level-dependent functional magnetic resonance imaging *Hum. Brain Mapp.* **34** 96–108

[36] Storti S F, Boscolo Galazzo I, Montemezzi S, Menegaz G and Pizzini F B 2017 Dual-echo ASL contributes to decrypting the link between functional connectivity and cerebral blow flow *Hum. Brain Mapp.* **38** 5831–44

[37] Storti S F, Galazzo I B, Pizzini F B and Menegaz G 2018 Dual-echo ASL based assessment of motor networks: a feasibility study *J. Neural. Eng.* **15** 26018

[38] Cohen A D, Nencka A S, Wang Y and Pillai J 2018 Multiband multi-echo simultaneous ASL/BOLD for task-induced functional MRI *PLoS One* **13** e0190427

[39] Tak S, Wang D J J, Polimeni J R, Yan L and Chen J J 2014 Dynamic and static contributions of the cerebrovasculature to the resting-state BOLD signal *Neuroimage* **84** 672–80

[40] Woolrich M W, Chiarelli P, Gallichan D, Perthen J and Liu T T 2006 Bayesian inference of hemodynamic changes in functional arterial spin labeling data *Magn. Reson. Med.* **56** 891–906
[41] Folstein M F 2010 *Mini-Mental State Examination MMSE-2; User's Manual* (Lutz, FL: PAR)
[42] Li Y T, Cercueil J-P, Yuan J, Chen W, Loffroy R and Wang Y X J 2017 Liver intravoxel incoherent motion (IVIM) magnetic resonance imaging: a comprehensive review of published data on normal values and applications for fibrosis and tumor evaluation *Quant. Imaging Med. Surg.* **7** 59–78
[43] Peirce J W 2007 PsychoPy—Psychophysics software in Python *J. Neurosci. Methods* **162** 8–13
[44] Wang J J, Fernandez-Seara M A, Wang S M and St Lawrence K S S 2007 When perfusion meets diffusion: *in vivo* measurement of water permeability in human brain *J. Cereb. Blood Flow Metab.* **27** 839–49
[45] Silva J P S, Mônaco L D M, Paschoal A M, Oliveira Í A F D and Leoni R F 2018 Effects of global signal regression and subtraction methods on resting-state functional connectivity using arterial spin labeling data *Magn. Reson. Imaging* **51** 151–7
[46] Oliveira Í A F, Guimaraes T M, Souza R M, dos Santos A C, Machado-de-Sousa J P, Hallak J E C and Leoni R F 2018 Brain functional and perfusional alterations in schizophrenia: an arterial spin labeling study *Psychiatry Res. Neuroimaging* **272** 71–78
[47] Wang Z 2012 Improving cerebral blood flow quantification for arterial spin labeled perfusion MRI by removing residual motion artifacts and global signal fluctuations *Magn. Reson. Imaging* **30** 1409–15
[48] Behzadi Y, Restom K, Liau J and Liu T T 2007 A component based noise correction method (CompCor) for BOLD and perfusion based fMRI *Neuroimage* **37** 90–101
[49] Bzdok D, Heeger A, Langner R, Laird A R, Fox P T, Palomero-Gallagher N, Vogt B A, Zilles K and Eickhoff S B 2015 Subspecialization in the human posterior medial cortex *Neuroimage* **106** 55–71
[50] RCoreTeam 2020 *R: A Language and Environment for Statistical Computing. Foundation for Statistical Computing* (available at: www.r-project.org/)
[51] Whitfield-Gabrieli S and Nieto-Castanon A 2012 Conn: a functional connectivity toolbox for correlated and anticorrelated brain networks *Brain Connect.* **2** 125–41
[52] Esposito F, Formisano E, Seifritz E, Goebel R, Morrone R, Tedeschi G and Di Salle F 2002 Spatial independent component analysis of functional MRI time-series: to what extent do results depend on the algorithm used? *Hum. Brain Mapp.* **16** 146–57
[53] Seghier M L 2008 Laterality index in functional MRI: methodological issues *Magn. Reson. Imaging* **26** 594–601
[54] de Martino F, Gentile F, Esposito F, Balsi M, Di Salle F, Goebel R and Formisano E 2007 Classification of fMRI independent components using IC-fingerprints and support vector machine classifiers *Neuroimage* **34** 177–94
[55] Ren Y, Nguyen V T, Guo L and Guo C C 2017 Inter-subject functional correlation reveal a hierarchical organization of extrinsic and intrinsic systems in the brain *Sci. Rep.* **7** 10876
[56] Muller A M and Meyer M 2014 Language in the brain at rest: new insights from resting state data and graph theoretical analysis *Front. Hum. Neurosci.* **8** 228
[57] Bassett D S and Bullmore E 2006 Small-world brain networks *Neuroscientist* **12** 512–23
[58] Mueller P A and Oppenheimer D M 2014 The pen is mightier than the keyboard: advantages of longhand over laptop note taking *Psychol. Sci.* **25** 1159–68
[59] Alaerts K, Geerlings F, Herremans L, Swinnen S P, Verhoeven J, Sunaert S, Wenderoth N and Zuo X-N 2015 Functional organization of the action observation network in autism: a graph theory approach *PLoS One* **10** e0137020
[60] Sporns O 2011 The non-random brain: efficiency, economy, and complex dynamics *Front. Comput. Neurosci.* **5** 5
[61] Rubinov M and Sporns O 2010 Complex network measures of brain connectivity: uses and interpretations *Neuroimage* **52** 1059–69
[62] Latora V and Marchiori M 2001 Efficient behavior of small-world networks *Phys. Rev. Lett.* **87** 198701
[63] Wang J, Zuo X and He Y 2010 Graph-based network analysis of resting-state functional MRI *Front. Syst. Neurosci.* **4** 16
[64] Wang Z, Aguirre G K, Rao H, Wang J, Fernandez-Seara M A, Childress A R and Detre J A 2008 Empirical optimization of ASL data analysis using an ASL data processing toolbox: ASLtbx *Magn. Reson. Imaging* **26** 261–9
[65] Warburton E, Wise R J S, Price C J, Weiller C, Hadar U, Ramsay S and Frackowiak R S J 1996 Noun and verb retrieval by normal subjects studies with PET *Brain* **119** 159–79
[66] Shuster L I and Lemieux S K 2005 An fMRI investigation of covertly and overtly produced mono- and multi-syllabic words *Brain Lang.* **93** 20–31
[67] Cutting L E, Clements A M, Courtney S, Rimrodt S L, Schafer J G, Bisesi J, Pekar J J and Pugh K R 2006 Differential components of sentence comprehension: beyond single word reading and memory *Neuroimage* **29** 429–38
[68] Dietz N A E, Jones K M, Gareau L, Zeffiro T A and Eden G F 2005 Phonological decoding involves left posterior fusiform gyrus *Hum. Brain Mapp.* **26** 81–93
[69] Papathanassiou D, Etard O, Mellet E, Zago L, Mazoyer B and Tzourio-Mazoyer N 2000 A common language network for comprehension and production: a contribution to the definition of language epicenters with PET *Neuroimage* **11** 347–57
[70] Olman C A, Davachi L, Inati S and García A V 2009 Distortion and signal loss in medial temporal lobe *PLoS One* **4** e8160
[71] Ischebeck A, Indefrey P, Usui N, Nose I, Hellwig F and Taira M 2004 Reading in a regular orthography: an FMRI study investigating the role of visual familiarity *J. Cogn. Neurosci.* **16** 727–41
[72] Kim J, Wasserman E A, Castro L and Freeman J H 2016 Anterior cingulate cortex inactivation impairs rodent visual selective attention and prospective memory *Behav. Neurosci.* **130** 75–90
[73] Paschoal A M, Paiva F F and Leoni R F 2019 Dual-echo arterial spin labeling for brain perfusion quantification and functional analysis *Concepts Magn. Reson. A* **2019** 5040465
[74] Liu T T and Wong E C 2005 A signal processing model for arterial spin labeling functional MRI *Neuroimage* **24** 207–15
[75] Costafreda S G, Fu C H Y, Lee L, Everitt B, Brammer M J and David A S 2006 A systematic review and quantitative appraisal of fMRI studies of verbal fluency: role of the left inferior frontal gyrus *Hum. Brain Mapp.* **27** 799–810
[76] Shapira-Lichter I, Oren N, Jacob Y, Gruberger M and Hendler T 2013 Portraying the unique contribution of the default mode network to internally driven mnemonic processes *Proc. Natl Acad. Sci. USA* **110** 4950–5
[77] O'Brien C P 2008 The CAGE questionnaire for detection of alcoholism: a remarkably useful but simple tool *JAMA* **300** 2054–6